Lebanese American University Repository (LAUR)

Post-print version/Author Accepted Manuscript

Publication metadata

Title: A numerical model for the solution of thermal elastohydrodynamic lubrication in coated circular contacts

Author(s): W. Habchi

Journal: Tribology International

DOI/Link: https://doi.org/10.1016/j.triboint.2014.01.002

How to cite this post-print from LAUR:

Habchi, W. (2014). A numerical model for the solution of thermal elastohydrodynamic lubrication in coated circular contacts. Tribology International, DOi: 10.1016/j.triboint.2014.01.002, URI: http://hdl.handle.net/10725/2173

© Year 2014

This Open Access post-print is licensed under a Creative Commons Attribution-Non Commercial-No Derivatives (CC-BY-NC-ND 4.0)

This paper is posted at LAU Repository

For more information, please contact: archives@lau.edu.lb

A Numerical Model for the Solution of Thermal Elastohydrodynamic Lubrication in Coated Circular Contacts

W. Habchi*

Lebanese American University, Department of Industrial and Mechanical Engineering, Byblos, Lebanon

*Corresponding author: wassim.habchi@lau.edu.lb

Abstract

This paper presents a finite element model for the solution of thermal elastohydrodynamic lubrication in coated circular contacts. The model is based on a full-system finite element resolution of the elastohydrodynamic and heat transfer equations. The effects of the coating's thermal and mechanical properties on lubrication performance are investigated. Two categories of surface coatings are considered based on thermal properties: high and low thermal inertia. It is found that low thermal inertia surface coatings act as insulators leading to a localized increase in the lubricant's temperature at the center of the contact. Therefore, friction can be significantly reduced while film thickness is barely affected. The opposite effect is observed for high thermal inertia coatings. These effects increase with coating's thickness.

Keywords: Thermal Elastohydrodynamic Lubrication; Surface Coatings; Finite Elements; Circular Contacts

1. Introduction

Surface coatings have been extensively used, for a long time now, to protect contacting surfaces in rotating machine elements from wear and fatigue. The addition of coatings to the surface of moving machine elements first came in the case of solid-to-solid dry contacts. In fact, a carefully selected thin surface coating with appropriate mechanical properties may be used to reduce the severity of the contact between surface asperities leading to reduced fatigue and wear and thus increased component life. Over the last few decades, the use of surface coatings has also extended to the case of lubricated machine elements. In particular, the elastohydrodynamic lubrication (EHL) of coated surfaces has gained increased attention as it was found from the earliest studies on the topic that surface coatings can significantly affect the lubricating performance of machine elements such as gears, bearings and cams which operate under elastohydrodynamic regime. One of the first attempts to model EHL contacts with coated surfaces was achieved by Bennett and Higginson [1] for the case of line contacts under isothermal Newtonian regime. Later, Elsharkawy and Hamrock [2] [3] introduced a numerical model for the solution of the EHL contact of a rigid cylinder with a rigid foundation coated by an

elastic layer also under isothermal Newtonian regime. These works studied the effects of the mechanical properties of the coatings and their thickness on pressure and film thickness distribution in EHL line contacts. It was found that hard coatings (coatings with a Young's modulus superior to that of the substrate), lead to higher pressure spikes than in the uncoated case where pressure spikes are also higher than the case of soft coatings (coatings with a Young's modulus inferior to that of the substrate). It was also found that the central pressure increases with the rigidity of the coating while the contact width is reduced. This effect was found to increase with the thickness of the coating. A central film thickness formula was even introduced for the case of coated line contacts lubricated by a non-Newtonian lubricant [4]. The solution of the three-dimensional case was out of reach until recently owing to limitations in computer power. One of the first studies dealing with circular EHL contacts with coated surfaces is that of Jin [5] [6]. Most of the cases mentioned so far are limited to the case of rigid substrates bonded to elastic coatings. The incorporation of the elasticity of the substrate into the analysis was done recently by Elsharkawy et al. [7] using the differential deflection method introduced by Holmes et al. [8] to evaluate the elastic deformation of the contacting solids. Liu et al. [9] [10] also incorporated the elasticity of the substrate in their analysis of coated EHL point contacts using the Discrete Convolution – Fast Fourier Transform method (DC-FFT) [11] to evaluate the elastic deflection of the contacting elements. The above mentioned studies on coated circular EHL contacts showed that coatings had the same effect on pressure and film thickness distribution as for the line contact case. That is, pressure spike height and central pressure increase with the rigidity of the coating while contact radius is reduced. As for line contacts, it was found that these effects increase with the coating's thickness.

All works mentioned so far assume isothermal conditions and focus on the effect of the rigidity of the coating and its thickness on pressure and film thickness in EHL contacts. The effect of the thermal properties of the coating on the lubrication performance of coated EHL contacts has earned very little attention. However, recent experimental works such as that of Evans et al. [12] or Björling et al. [13] reported significantly reduced friction (up to 50%) in DLC-coated EHL contacts. In [13], based on a simplified analytical estimation of the temperature increase in the lubricant film induced by the DLC surface coating, the authors suggested that the observed friction reduction might be a thermal phenomenon. This hypothesis was later verified in [14] by validating the friction measurements against numerical predictions obtained using the full-system finite element approach [15] [16]. In [14], only thin 2μm DLC coatings were considered which had very little influence on the elastohydrodynamic part of the solution but a significant effect on the thermal part. It was shown that this type of coating, which has a relatively low thermal inertia, prevents heat from being diffused from the center of the contact towards the peripheral area and the solids. Thus, a local increase in the temperature of the lubricant film at the center of the contact is observed. This local increase in temperature leads to reduced friction with very little effect on film thickness since the lubricant's temperature at the inlet of the contact is barely affected. In fact, the thermal inertia I of a given material is defined as $I = \sqrt{k\,\rho\,c} = \sqrt{k\,C}$, where C is the volumetric heat capacity of the material and k its thermal

conductivity. Thus a high thermal inertia material usually has a high thermal conductivity and volumetric heat capacity. As such, it has a high ability to transport heat by conduction and advection respectively. In fact, the thermal conductivity of a material represents its ability to transport heat by conduction while its volumetric heat capacity represents its ability to store and transport heat by advection (heat transfer by mass). On the other hand, a low thermal inertia material has a low ability to transport heat by conduction and advection, and thus it acts as an insulating material. The coating's thickness being very thin (2μm), the effect of the coating was only included in the thermal part of the numerical model while in the EHL part uncoated surfaces were considered.

Based on the above, it is obvious that the lubrication performance of thermal elastohydrodynamic (TEHD) contacts can be controlled through an adequate choice of surface coatings that is not only based on their mechanical properties but also on their thermal properties. The latter have a significant impact on friction in coated EHD contacts. The author believes that this topic deserves being further investigated in detail. The current paper presents a numerical model for the solution of coated TEHD circular contacts incorporating surface coatings in both the EHL and thermal parts of the model. This model is used to run a comprehensive investigation of the effects of the mechanical properties as well as the thermal properties of the coating on the lubrication performance of TEHD circular contacts in terms of pressure, film thickness as well as friction. Next, the numerical model employed in this work is described in detail.

2. Model description

In this section, the numerical model for coated TEHD circular contacts developed in this work is described in detail. The model is based on the full-system finite element approach introduced in [15] [16] for uncoated EHD contacts. The geometry of a circular EHD contact can be reduced to that of a contact between a plane and a ball of radius R as shown in figure 1. In the current work, a layer of coating is added to the surface of both the plane and ball. It is assumed that the substrates of the two contacting bodies are made of the same material. As for the coatings, they are assumed to be bonded to the substrates and both surface coatings are also assumed to be made of the same material. Both the substrates and coatings are considered to be perfectly elastic. The surfaces of the plane and ball are assumed to be smooth and moving at constant unidirectional surface speeds u_p and u_b respectively in the x-direction. The contact is subject to an external applied load F and a fully-flooded regime is assumed. The lubricant is assumed to have a generalized-Newtonian behavior.

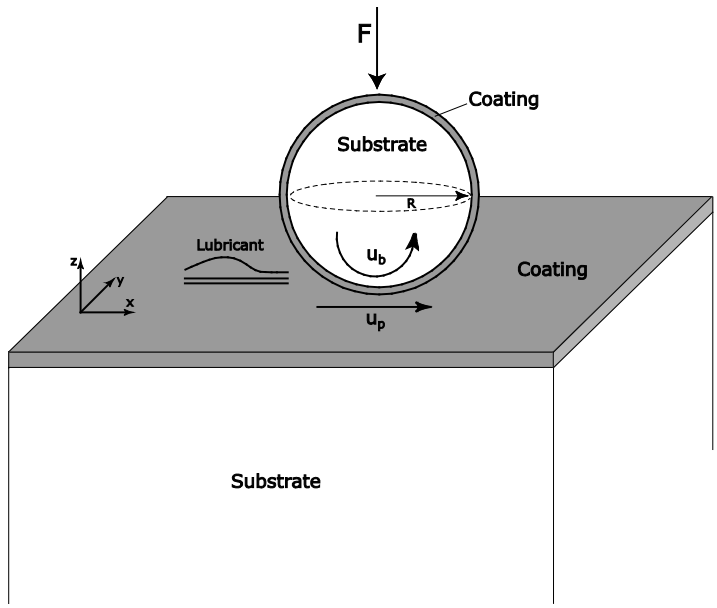

Figure 1: Geometry of the coated TEHD circular contact

The numerical model for coated circular TEHD contacts can be split into two parts: the elastohydrodynamic part describing the hydrodynamic flow of the lubricant into the contact as well as the elastic deformation of the contacting solids and the thermal part describing heat transfer between the lubricant film and the solids.

2.1. Elastohydrodynamic model

The elastohydrodynamic model is governed by three main equations: generalized-Reynolds, linear elasticity and load balance equations. Before going into the details of these equations, the definition of the following dimensionless parameters is due first:

$$
\begin{aligned}
&P = \frac{p}{p_h}, \quad \bar{\eta} = \frac{\eta}{\mu_R}, \quad \bar{\rho} = \frac{\rho}{\rho_R} \\
&U = \frac{uR}{a^2}, \quad V = \frac{vR}{a^2}, \quad W = \frac{wR}{a^2}, \quad H = \frac{hR}{a^2} \\
&X = \frac{x}{a}, \quad Y = \frac{y}{a}, \quad Z = \begin{cases} \dfrac{z}{a}: \text{ Substrate} \\ \dfrac{z}{t_c}: \text{ Coatings} \end{cases}
\end{aligned}
\tag{1}
$$

Where a and p_h correspond to the uncoated Hertzian contact radius and pressure respectively (evaluated based on the substrate's mechanical properties), t_c corresponds to the coating's thickness, ρ_R and μ_R correspond respectively to the density and low-shear viscosity of the lubricant at a reference state, η is the generalized Newtonian viscosity and u, v and w are the x, y and z-components respectively of the total elastic deformation of the solids. The use of the

above definition of Z allows defining a unique geometrical domain of unit dimensionless thickness for the coating irrespective of its actual thickness t_c. The dimensionless computational domain for the EHL part is shown in figure 2. In [16] it was shown that a cube of dimensionless side length of 60 may be used to approximate a half-space used here for the elastic deformation calculation of the substrate. A coating layer of unit dimensionless thickness is added to the surface of the substrate as shown in figure 2. The symmetry of the problem with respect to the *xz*-plane is taken into consideration in order to simplify the model and reduce the computational overhead. The pressure distribution in the two-dimensional contact area Ω_c located on the cube's surface is governed by the generalized Reynolds equation given by Yang and Wen [17]:

$$\frac{\partial}{\partial X}\left(\bar{\varepsilon}\,\frac{\partial P}{\partial X}\right)+\frac{\partial}{\partial Y}\left(\bar{\varepsilon}\,\frac{\partial P}{\partial Y}\right)-\frac{\partial\left(\bar{\rho}^{*}H\right)}{\partial X}=0 \qquad (2)$$

$$\bar{\varepsilon}=\left(\frac{\bar{\rho}}{\bar{\eta}}\right)_e\frac{H^3}{\lambda} \qquad \left(\frac{\bar{\rho}}{\bar{\eta}}\right)_e=\frac{\bar{\eta}_e\bar{\rho}'_e}{\bar{\eta}'_e}-\bar{\rho}''_e \qquad \lambda=\frac{u_m R^2\mu_R}{a^3 p_h} \quad \text{with} \quad u_m=\frac{u_p+u_b}{2}$$

Where:

$$\bar{\rho}^{*}=\frac{\left[\bar{\rho}'_e\bar{\eta}_e\left(u_b-u_p\right)+\bar{\rho}_e u_p\right]}{u_m} \qquad \bar{\rho}_e=\int_0^1\bar{\rho}\,dZ$$

$$\bar{\rho}'_e=\int_0^1\bar{\rho}\int_0^Z\frac{dZ'}{\bar{\eta}}dZ \qquad \bar{\rho}''_e=\int_0^1\bar{\rho}\int_0^Z\frac{Z'dZ'}{\bar{\eta}}dZ$$

$$\frac{1}{\bar{\eta}_e}=\int_0^1\frac{dZ}{\bar{\eta}} \qquad \frac{1}{\bar{\eta}'_e}=\int_0^1\frac{Z\,dZ}{\bar{\eta}}$$

As suggested in classical numerical EHL [18], the geometrical domain of the contact area Ω_c (considering the symmetry of the problem with respect to the xz-plane) is taken to be $-4.5\le X\le 1.5$ and $-3.0\le Y\le 0.0$, to ensure that the pressure is nil at the inlet and exit boundaries of the domain. Note that this equation accounts for the variations of density and viscosity across the film thickness through the integral terms. In fact, the changes in density are due to temperature variations across the lubricant film whereas the changes in viscosity stem from both temperature and shear rate variations across the film. Moreover, both density and viscosity are allowed to vary with pressure and temperature throughout the lubricant film. A zero pressure boundary condition is imposed on the boundaries of Ω_c and the penalty method proposed by Wu [19] is used to handle the free cavitation boundary arising at the contact exit. The latter consists in adding a penalty term ($-\xi\,P^{-}$) to the generalized Reynolds equation, where ξ is a large positive number and P^{-} corresponds to the negative part of the pressure domain. This term only acts in the negative pressure regions, where; provided ξ is sufficiently large; it dominates Reynolds' equation and forces the negative pressures arising in the solution towards zero. The dimensionless film thickness H in equation (2) is expressed as:

$$H\left(X,Y\right)=H_0+\frac{X^2+Y^2}{2}-W\left(X,Y\right) \qquad (3)$$

Where H_0 is a constant and $W(X,Y)$ is the dimensionless *z*-component distribution of the total elastic deflection of the ball and plane over the contact zone Ω_c. The latter is obtained by applying the linear elasticity equations to the contacting solids. The linear elasticity model may be simplified to an equivalent one where one of the contacting bodies (substrate + coating) is rigid while the other is elastic and accommodates the total elastic deflection of both solid components. In the current case, since the two solids are made of the same material and their coatings too; according to [16]; the equivalent elastic material properties would reduce to:

$$\begin{aligned} &\text{Substrate:} \quad E_{s,eq} = \frac{E_s}{2} \quad \text{and} \quad \upsilon_{s,eq} = \upsilon_s \\ &\text{Coating:} \quad E_{c,eq} = \frac{E_c}{2} \quad \text{and} \quad \upsilon_{c,eq} = \upsilon_c \end{aligned} \tag{4}$$

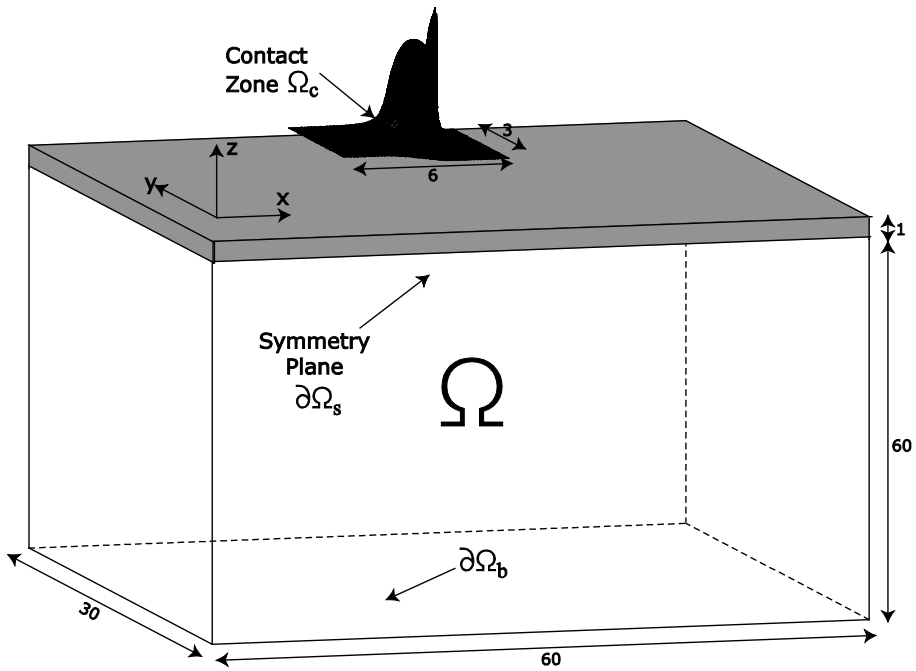

Figure 2: Computational domain of the EHD model for coated circular contacts

The elastic deflection of the contacting solids is obtained by applying the three-dimensional linear elasticity equations to the equivalent substrate and coating defined by the equivalent dimensionless geometrical domain provided in figure 2. The detailed derivation of these equations is provided in Appendix A. In dimensionless form, after simplification, these equations read:

$$
\text{Substrate:}\quad \begin{cases}
\dfrac{\partial}{\partial X}\left[\left(\lambda_s+2\mu_s\right)\dfrac{\partial U}{\partial X}+\lambda_s\dfrac{\partial V}{\partial Y}+\lambda_s\dfrac{\partial W}{\partial Z}\right] \\
\qquad\qquad +\dfrac{\partial}{\partial Y}\left[\mu_s\left(\dfrac{\partial U}{\partial Y}+\dfrac{\partial V}{\partial X}\right)\right]+\dfrac{\partial}{\partial Z}\left[\mu_s\left(\dfrac{\partial U}{\partial Z}+\dfrac{\partial W}{\partial X}\right)\right]=0 \\
\dfrac{\partial}{\partial X}\left[\mu_s\left(\dfrac{\partial U}{\partial Y}+\dfrac{\partial V}{\partial X}\right)\right]+\dfrac{\partial}{\partial Y}\left[\lambda_s\dfrac{\partial U}{\partial X}+\left(\lambda_s+2\mu_s\right)\dfrac{\partial V}{\partial Y}+\lambda_s\dfrac{\partial W}{\partial Z}\right] \\
\qquad\qquad +\dfrac{\partial}{\partial Z}\left[\mu_s\left(\dfrac{\partial V}{\partial Z}+\dfrac{\partial W}{\partial Y}\right)\right]=0 \\
\dfrac{\partial}{\partial X}\left[\mu_s\left(\dfrac{\partial U}{\partial Z}+\dfrac{\partial W}{\partial X}\right)\right]+\dfrac{\partial}{\partial Y}\left[\mu_s\left(\dfrac{\partial V}{\partial Z}+\dfrac{\partial W}{\partial Y}\right)\right] \\
\qquad\qquad +\dfrac{\partial}{\partial Z}\left[\lambda_s\dfrac{\partial U}{\partial X}+\lambda_s\dfrac{\partial V}{\partial Y}+\left(\lambda_s+2\mu_s\right)\dfrac{\partial W}{\partial Z}\right]=0
\end{cases} \tag{5a}
$$

$$
\text{Coating:}\quad \begin{cases}
\dfrac{\partial}{\partial X}\left[\left(\lambda_c+2\mu_c\right)\dfrac{t_c}{a}\dfrac{\partial U}{\partial X}+\lambda_c\dfrac{t_c}{a}\dfrac{\partial V}{\partial Y}+\lambda_c\dfrac{\partial W}{\partial Z}\right] \\
\qquad\qquad +\dfrac{\partial}{\partial Y}\left[\mu_c\dfrac{t_c}{a}\left(\dfrac{\partial U}{\partial Y}+\dfrac{\partial V}{\partial X}\right)\right]+\dfrac{\partial}{\partial Z}\left[\mu_c\left(\dfrac{a}{t_c}\dfrac{\partial U}{\partial Z}+\dfrac{\partial W}{\partial X}\right)\right]=0 \\
\dfrac{\partial}{\partial X}\left[\mu_c\dfrac{t_c}{a}\left(\dfrac{\partial U}{\partial Y}+\dfrac{\partial V}{\partial X}\right)\right]+\dfrac{\partial}{\partial Y}\left[\lambda_c\dfrac{t_c}{a}\dfrac{\partial U}{\partial X}+\left(\lambda_c+2\mu_c\right)\dfrac{t_c}{a}\dfrac{\partial V}{\partial Y}+\lambda_c\dfrac{\partial W}{\partial Z}\right] \\
\qquad\qquad +\dfrac{\partial}{\partial Z}\left[\mu_c\left(\dfrac{a}{t_c}\dfrac{\partial V}{\partial Z}+\dfrac{\partial W}{\partial Y}\right)\right]=0 \\
\dfrac{\partial}{\partial X}\left[\mu_c\left(\dfrac{\partial U}{\partial Z}+\dfrac{t_c}{a}\dfrac{\partial W}{\partial X}\right)\right]+\dfrac{\partial}{\partial Y}\left[\mu_c\left(\dfrac{\partial V}{\partial Z}+\dfrac{t_c}{a}\dfrac{\partial W}{\partial Y}\right)\right] \\
\qquad\qquad +\dfrac{\partial}{\partial Z}\left[\lambda_c\dfrac{\partial U}{\partial X}+\lambda_c\dfrac{\partial V}{\partial Y}+\left(\lambda_c+2\mu_c\right)\dfrac{a}{t_c}\dfrac{\partial W}{\partial Z}\right]=0
\end{cases} \tag{5b}
$$

Where $\left(\lambda_s,\upsilon_s\right)$ and $\left(\lambda_c,\upsilon_c\right)$ are the Lamé parameters for the substrate's and coating's material respectively. These are defined as:

$$
\begin{aligned}
&\text{Substrate:} \qquad \lambda_s=\frac{\upsilon_{s,eq}E_{s,eq}}{\left(1+\upsilon_{s,eq}\right)\left(1-2\upsilon_{s,eq}\right)} \quad , \quad \mu_s=\frac{E_{s,eq}}{2\left(1+\upsilon_{s,eq}\right)} \\
&\text{Coating:} \qquad \lambda_c=\frac{\upsilon_{c,eq}E_{c,eq}}{\left(1+\upsilon_{c,eq}\right)\left(1-2\upsilon_{c,eq}\right)} \quad , \quad \mu_c=\frac{E_{c,eq}}{2\left(1+\upsilon_{c,eq}\right)}
\end{aligned} \tag{6}
$$

Note that according to equations (5a) and (5b), the use of the equivalent material properties defined in equation (4) leads to a total elastic deformation that is twice that of each solid body (substrate + coating) taken separately. This is to be expected since both substrates are made of

the same material and their coatings too and they are subject to the same loading conditions. Equations (5) are associated with the following boundary conditions:

$$\begin{cases} \bar{\sigma}_{\mathrm{n}} = \bar{\sigma} \cdot \vec{n} = \bar{\sigma}_{ZZ} = \lambda_c \dfrac{\partial U}{\partial X} + \lambda_c \dfrac{\partial V}{\partial Y} + \left(\lambda_c + 2\mu_c\right) \dfrac{a}{t_c} \dfrac{\partial W}{\partial Z} = -\dfrac{P\,R\,p_h}{a} & \text{on } \Omega_{\mathrm{c}} \\ U = V = W = 0 & \text{on } \partial\Omega_{\mathrm{b}} \\ V = 0 & \text{on } \partial\Omega_{\mathrm{s}} \text{ (Symmetry)} \\ \bar{\sigma}_{\mathrm{n}} = 0 & \text{elsewhere} \end{cases} \tag{7}$$

And a continuity boundary condition is imposed on the common boundary between the substrate and coating domains. Finally, the last equation needed to complete the elastohydrodynamic part is the load balance equation which; considering the symmetry of the problem; can be written in dimensionless form as:

$$\int_{\Omega_c} P\left(X, Y\right) d\Omega = \frac{\pi}{3} \tag{8}$$

This equation stems from an equilibrium of forces applied in the z-direction to the contacting solids. It is used to ensure that the correct external load F is applied to the contact by monitoring the value of the film thickness constant term H_0. Equations (1)-(8) completely define the elastohydrodynamic part of the model. The unknowns of these equations are: the dimensionless pressure distribution P, the dimensionless elastic deformations U, V and W and the film thickness constant term H_0.

2.2. Thermal model

The thermal part is based on the heat transfer equation applied to the lubricant and contacting solids. In this part, slightly different dimensionless parameters are defined for the space coordinates:

$$X = \frac{x}{a}\,,\; Y = \frac{y}{a}\,,\; Z = \begin{cases} z/a & : \text{substrates} \\ z/t_c & : \text{coatings} \\ z/h & : \text{lubricant} \end{cases} \tag{9}$$

The use of the above definition of Z allows defining unique geometrical domains of unit dimensionless thickness for the coatings and the lubricant irrespective of the actual thickness t_c of the coating or the actual lubricant film thickness h. The geometrical domain for the thermal problem is shown in Figure 3. Note that the symmetry of the problem with respect to the xz-plane is also taken into consideration for the thermal part. Kaneta et al. [20] and Wang et al. [21] showed that for the contacting solids, in most cases, a dimensionless depth of 3.15 is sufficient to ensure a zero temperature gradient in regions far from the contact surface. Therefore, this depth is adopted for the substrates in the current work.

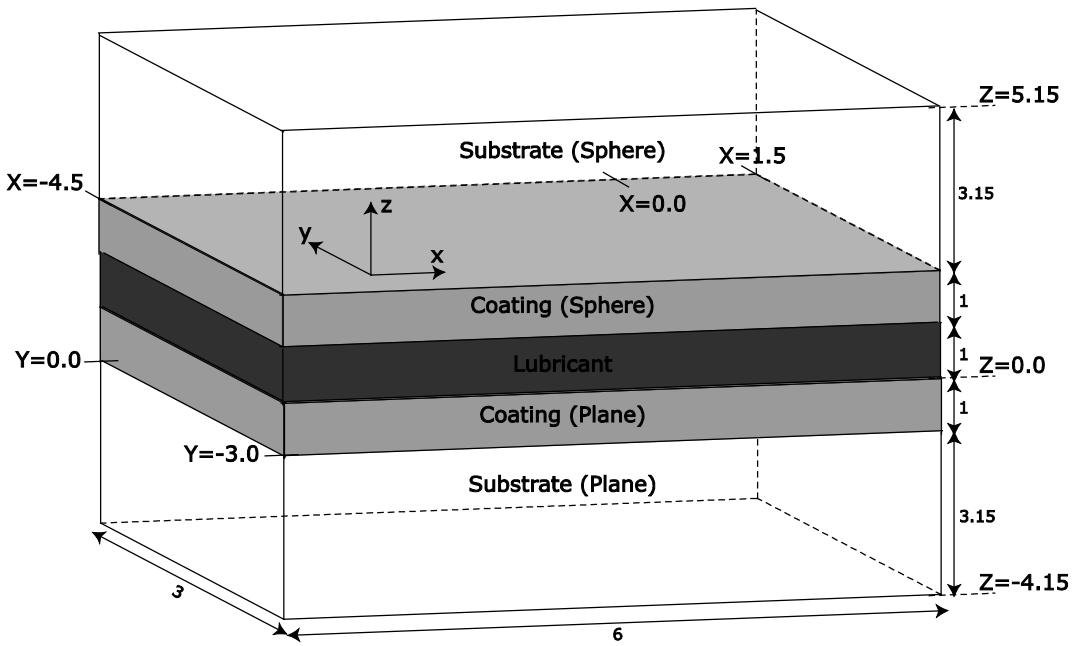

Figure 3: Computational domain of the thermal model for coated circular contacts

The thermal model consists in applying the three-dimensional heat transfer equation to the solids (substrates and coatings) and the lubricant domain. As a consequence of the relatively small dimension of the lubricant film in the *z*-direction compared to the *x* and *y*-directions, many works such as [22] [23] [24] [25] have shown that in the lubricant film, heat convection in the *z*-direction as well as heat conduction in the *x* and *y*-directions can be neglected compared to convection in the *x* and *y* directions and conduction in the *z*-direction respectively. Thus, after simplification, the heat transfer equations applied to the solids and lubricant film may be written in dimensionless form as:

$$\begin{cases} -\dfrac{\partial}{\partial X}\left(\dfrac{k_s}{a}\dfrac{\partial T}{\partial X}\right)-\dfrac{\partial}{\partial Y}\left(\dfrac{k_s}{a}\dfrac{\partial T}{\partial Y}\right)-\dfrac{\partial}{\partial Z}\left(\dfrac{k_s}{a}\dfrac{\partial T}{\partial Z}\right)+\rho_s c_s u_b\left(\dfrac{\partial T}{\partial X}\right)=0 & \text{(Ball Substrate)} \\ -\dfrac{\partial}{\partial X}\left(\dfrac{k_c t_c}{a^2}\dfrac{\partial T}{\partial X}\right)-\dfrac{\partial}{\partial Y}\left(\dfrac{k_c t_c}{a^2}\dfrac{\partial T}{\partial Y}\right)-\dfrac{\partial}{\partial Z}\left(\dfrac{k_c}{t_c}\dfrac{\partial T}{\partial Z}\right)+\rho_c c_c u_b\dfrac{t_c}{a}\left(\dfrac{\partial T}{\partial X}\right)=0 & \text{(Ball Coating)} \\ -\dfrac{\partial}{\partial Z}\left(\dfrac{kR}{Ha^2}\dfrac{\partial T}{\partial Z}\right)+\rho_R\bar{\rho}\,c\dfrac{Ha}{R}\left(u_f\dfrac{\partial T}{\partial X}+v_f\dfrac{\partial T}{\partial Y}\right)=Q_{comp}+Q_{shear} & \text{(Lubricant film)} \\ -\dfrac{\partial}{\partial X}\left(\dfrac{k_c t_c}{a^2}\dfrac{\partial T}{\partial X}\right)-\dfrac{\partial}{\partial Y}\left(\dfrac{k_c t_c}{a^2}\dfrac{\partial T}{\partial Y}\right)-\dfrac{\partial}{\partial Z}\left(\dfrac{k_c}{t_c}\dfrac{\partial T}{\partial Z}\right)+\rho_c c_c u_p\dfrac{t_c}{a}\left(\dfrac{\partial T}{\partial X}\right)=0 & \text{(Plane Coating)} \\ -\dfrac{\partial}{\partial X}\left(\dfrac{k_s}{a}\dfrac{\partial T}{\partial X}\right)-\dfrac{\partial}{\partial Y}\left(\dfrac{k_s}{a}\dfrac{\partial T}{\partial Y}\right)-\dfrac{\partial}{\partial Z}\left(\dfrac{k_s}{a}\dfrac{\partial T}{\partial Z}\right)+\rho_s c_s u_p\left(\dfrac{\partial T}{\partial X}\right)=0 & \text{(Plane Substrate)} \end{cases} \quad (10)$$

Where: $Q_{comp}=-\dfrac{T}{\bar{\rho}}\dfrac{\partial\bar{\rho}}{\partial T}p_h\dfrac{Ha}{R}\left(u_f\dfrac{\partial P}{\partial X}+v_f\dfrac{\partial P}{\partial Y}\right)$ and $Q_{shear}=\dfrac{\bar{\eta}\mu_R R}{Ha^2}\left[\left(\dfrac{\partial u_f}{\partial Z}\right)^2+\left(\dfrac{\partial v_f}{\partial Z}\right)^2\right]$

The terms Q_{comp} and Q_{shear} correspond to the compressive heating/cooling and shear heating source terms respectively. Note the appearance of the Hertzian contact radius *a*, the coating thickness t_c and the lubricant's film thickness $h = Ha^2/R$ in the different equations owing to the different definitions of the dimensionless space coordinate *Z* in the thermal model as suggested by equation (9). The lubricant velocity field components u_f and v_f in the *x* and *y*-directions respectively are defined as:

$$\begin{cases} u_f = \dfrac{\partial p}{\partial x}\left(\displaystyle\int_0^z \frac{z}{\eta}dz - \frac{\eta_e}{\eta_e'}\int_0^z \frac{dz}{\eta}\right) + \eta_e\left(u_b - u_p\right)\displaystyle\int_0^z \frac{dz}{\eta} + u_p \\ v_f = \dfrac{\partial p}{\partial y}\left(\displaystyle\int_0^z \frac{z}{\eta}dz - \frac{\eta_e}{\eta_e'}\int_0^z \frac{dz}{\eta}\right) \end{cases} \tag{11}$$

Note that $\eta_e = \mu_R \times \overline{\eta}_e$ and $\eta_e' = \mu_R \times \overline{\eta}_e'$ where $\overline{\eta}_e$ and $\overline{\eta}_e'$ are the integral terms defined in equation (2). The transport properties as well as the thermal properties of the lubricant are allowed to vary with temperature and pressure across the lubricant film. The importance of accounting for the dependence of the thermal properties of the lubricant on temperature and pressure has been thoroughly discussed in [26] and [27]. In fact, it was shown that neglecting the variations of the lubricant's thermal properties with pressure and temperature leads to an underestimation of friction at high sliding speeds. To complete the thermal model, equations (10) are associated with the following boundary conditions:

$$\begin{cases} T\left(X = -4.5, Y, -4.15 \le Z \le 0.0\right) = T\left(X = -4.5, Y, 1.0 \le Z \le 5.15\right) = T_0 \\ T\left(X, Y, Z = -4.15\right) = T\left(X, Y, Z = 5.15\right) = T_0 \\ T\left(X = -4.5, Y, 0.0 \le Z \le 1.0\right) = T_0 \qquad \text{where} \quad \mathrm{u}_f \ge 0 \end{cases} \tag{12}$$

Note that boundary conditions are only required at inlet boundaries due to the hyperbolic character of equations (10). Also note that zero heat flux (symmetry) boundary conditions are applied to the symmetry plane *xz* and that heat flux continuity boundary conditions are imposed at all substrate-coating and coating-lubricant interfaces. Equations (10)-(12) completely define the thermal part of the TEHL model for coated circular contacts. The unknown of this thermal part is the temperature distribution *T* in the solids (substrates + coatings) and the lubricant film.

2.3. Overall numerical procedure

The overall numerical procedure summarized by the flow chart of figure 4 consists in solving the EHD and thermal parts separately and establishing an iterative procedure between their respective solutions until overall convergence is attained. All equations are discretized through a finite element (FEM) procedure using a commercial software: COMSOL Multiphysics [28]. A TEHD custom-tailored mesh is employed as detailed in [16]; that is, a non-regular non-structured tetrahedral mesh is employed for both the EHD and thermal parts. The mesh is fine in the contact region (with a maximum allowed edge size for tetrahedral elements of 0.05) and its size is

gradually increased with the distance from the center of the contact. Note that both linear elasticity and heat transfer equations were written in such a way that continuity of stresses across the substrate-coating interface and heat fluxes across the substrate-coating and coating-lubricant interfaces respectively is automatically satisfied by setting to zero the boundary integral terms arising in the weak form FEM formulation of equations (5) and (10) at these interfaces. Numerical details pertaining to the FEM solution of the different equations are omitted here for brevity and only the main features of the model are recalled. For more details, the interested reader is referred to [16]. In addition, an extensive series of mesh-independence and model validation tests have been carried out. The details of these tests have also been omitted here for brevity.

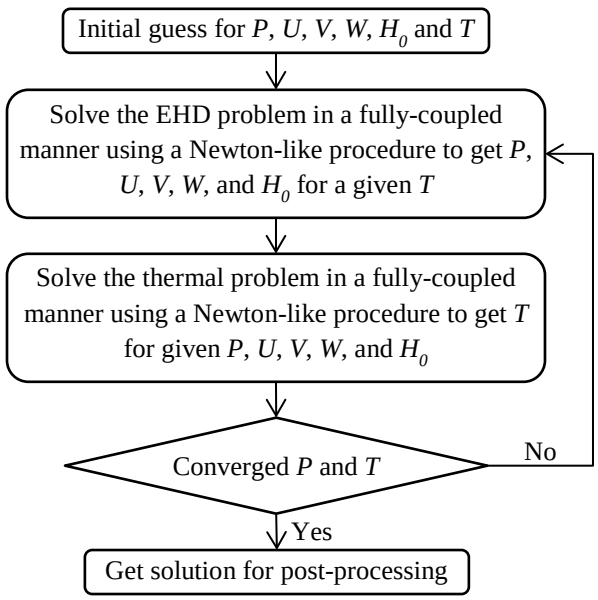

Figure 4: Flow chart of the overall iterative numerical procedure

The starting point for the overall numerical procedure is the selection of an appropriate initial guess for the pressure distribution P. In the current work, a modified dimensionless Hertzian pressure distribution is used taking into consideration the classical observations found in the literature [7] [9] [10] pertaining to the increase in central pressure and decrease in contact width with the rigidity of the coating and the increase in both effects with the thickness of the coating. The initial guess for P is taken to be:

$$P = \begin{cases} \theta\sqrt{1-\theta\left(X^2+Y^2\right)} & \text{for} \quad X^2+Y^2 \le \dfrac{1}{\theta} \\ 0 & \text{elsewhere} \end{cases} \qquad (13)$$

Note that in the above equation, θ corresponds to the modified dimensionless Hertzian pressure while $\sqrt{1/\theta}$ corresponds to the modified dimensionless Hertzian contact radius. The value of θ is chosen to be greater than unity for hard coatings and smaller than unity for soft coatings and the deviation of θ from unity is increased with the coating's thickness. Note that for

θ = 1, equation (13) corresponds to the classical dimensionless Hertzian pressure distribution used as an initial guess for uncoated cases or cases where the coating's mechanical properties are the same as those of the substrate. The elastic deformation corresponding to this modified dimensionless Hertzian pressure distribution is used as the initial guess for U, V, and W. As for the initial guess for the temperature distribution T, a uniform temperature distribution $T=T_0$ is chosen for the substrates, coatings and lubricant film where T_0 is the ambient temperature.

First, for the EHD part, starting from the initial guess for pressure P, elastic deformation components U, V and W and film thickness constant parameter H_0; the nonlinear system of equations (2), (5) and (8) is solved in a fully-coupled manner using a Newton-like nonlinear resolution procedure to determine P, U, V, W and H_0 for a given temperature distribution T. Equation (2) is applied to the two-dimensional contact zone Ω_c whereas equations (5) are applied to the three-dimensional solid domain shown in figure 2. Equation (8) which is an ordinary integral equation is directly added to the system of equations formed by equations (2) and (5) and is associated with an additional unknown H_0. Special stabilized formulations are employed for the solution of the generalized Reynolds equation at high loads as suggested in [16]. Lagrange fifth order elements are employed for Reynolds equation whereas second order elements are used for the linear elasticity equations. This allows an increased precision required for the solution of the two-dimensional Reynolds equation without inducing any unnecessary increase in the number of degrees of freedom (dofs) of the three-dimensional linear elasticity part.

Then, for the thermal part, starting from the initial guess for the temperature distribution T; the nonlinear system of equations (10) is solved in a fully-coupled manner also using a Newton-like nonlinear resolution procedure to determine T in the solids and lubricant film for given P, U, V, W distributions and H_0 obtained from the EHD part. Lagrange second order elements are employed for the thermal part and special stabilized formulations are also used for the solution of equations (10) under convection-dominated regime as suggested in [16].

The above process is repeated and an iterative procedure is established between the respective solutions of the EHD and thermal problems until overall convergence is attained as described in the flow chart of figure 4. Note that at every iteration, the initial guesses for P, U, V, W, H_0 and T are updated to their respective solutions at the previous iteration.

3. Results

The lubricant selected for the numerical experiments of this section is Shell T9, a mineral oil for which the transport and thermal properties have been thoroughly characterized in [26]. In the following, subscripts 0 and R indicate, respectively, ambient pressure and temperature (p_0 = 0 and $T_0 = 30^o\mathrm{C}$) and a reference state ($p_R = 0$ and $T_R = 25^o\mathrm{C}$). Density variations with pressure and temperature are described by the Murnaghan [29] equation of state:

$$\rho = \frac{\rho_R}{1 + a_V\left(T - T_R\right)} \times \left(1 + \frac{K_0'}{K_0}p\right)^{\frac{1}{K_0'}} \quad \text{with} \quad K_0 = K_{00}\exp\left(-\beta_K T\right) \qquad (14)$$

Where $K_0' = 10.545$, $a_V = 7.734\times10^{-4}\ \mathrm{K}^{-1}$, $K_{00} = 9.234\ \mathrm{GPa}$, $\rho_R = 875\,Kg/m^3$ and $\beta_K = 6.090\times10^{-3}\ \mathrm{K}^{-1}$. The low-shear viscosity dependence on temperature and pressure is described by a Vogel-like model [30] [31]:

$$\mu = \mu_\infty \exp\left(\frac{B_F \varphi_\infty}{\varphi - \varphi_\infty}\right) \quad \text{with} \quad \varphi = \left(\frac{T}{T_R}\right)\left(\frac{V}{V_R}\right)^g \qquad (15)$$

Where $g = 5.0348$, $\varphi_\infty = 0.26844$, $B_F = 12.898$, and $\mu_\infty = 1.489\times10^{-4}\ \mathrm{Pa\cdot s}$. And from the Murnaghan equation of state:

$$\frac{V}{V_R} = \frac{1 + a_V\left(T - T_R\right)}{\left(1 + \frac{K_0'}{K_0}p\right)^{1/K_0'}} \qquad (16)$$

Note that the low-shear viscosity at the reference state $\mu_R = 0.0135\ \mathrm{Pa.s}$. For the shear dependence of viscosity, the single-Newtonian modified Carreau-Yasuda equation [32] is used to describe the dependence of the generalized viscosity η on shear stress τ:

$$\eta = \frac{\mu}{\left[1 + \left(\frac{\tau}{G}\right)^a\right]^{\frac{\frac{1}{n}-1}{a}}} \qquad (17)$$

Where $G = 7.0\ \mathrm{MPa}$, $a = 5$ and $n = 0.35$. As for the limiting-shear-stress τ_L of Shell T9 lubricant, a linear dependence on pressure is used:

$$\tau_L = \Lambda\ p \qquad (18)$$

Where the limiting stress-pressure coefficient $\Lambda = 0.083$. The dependence of the thermal conductivity k of Shell T9 on pressure and temperature is given by the following relationship [26]:

$$k = B_k + C_k \kappa^{-s} \quad \text{with} \quad \kappa = \left(\frac{V}{V_R}\right)\left[1 + A\left(\frac{T}{T_R}\right)\left(\frac{V}{V_R}\right)^3\right] \qquad (19)$$

Where $A = -0.101$, $B_k = 0.053\ \mathrm{W/m\cdot K}$, $C_k = 0.026\ \mathrm{W/m\cdot K}$ and $s = 7.6$. And finally, the dependence of the volumetric heat capacity $C = \rho c$ on pressure and temperature is given by the following relationship [26]:

$$C = C' + m\chi \quad \text{with} \quad \chi = \left(\frac{T}{T_R}\right)\left(\frac{V}{V_R}\right)^{-4} \qquad (20)$$

Where $C' = 1.17\times10^6\ J/m^3\cdot K$ and $m = 0.39\times10^6\ \mathrm{J/m^3\cdot K}$. The operating conditions and solid material properties are summarized in Table 1. Two loads are considered 25N and 100N which corresponding non-coated Hertzian pressures are 0.74GPa and 1.17GPa respectively. Note that the substrate is made of steel and that coatings are classified in two thermal categories based on their thermal inertia $I = \sqrt{k\,\rho\,c}$ (low and high thermal inertia). Numerical experiments are run under both pure-rolling and rolling-sliding conditions for slide-to-roll ratios (*SRR*) ranging from 0 to 50%.

Operating conditions	Solid material properties			
T_0=30ºC	Substrate	Coatings		
u_m=1m/s	E_s=210GPa	Mechanical properties	Thermal properties	
SRR=0.0-0.5	υ_s=0.3		Low thermal inertia	High thermal inertia
F=25;100N	ρ_s=7850kg/m^3	E_c=52.5;105;210;420GPa	ρ_c=3500kg/m^3	ρ_c=10000kg/m^3
R=12.7mm	k_s=46W/m.K	υ_c=0.3	k_c=5W/m.K	k_c=90W/m.K
t_c=20;40;80;160µm	c_s=470J/kg.K		c_c=200J/kg.K	c_c=1000J/kg.K

Table 1: Operating conditions and solid material properties

Next, the effect of the coating's mechanical and thermal properties on the performance of coated TEHL circular contacts is investigated.

3.1. Effect of coating mechanical properties

In this section, the effects of the coating's mechanical properties on dimensionless pressure and film thickness in coated TEHD circular contacts are investigated. In order to isolate the effects of mechanical properties on lubricating performance, thermal properties of the coating are taken to be those of the substrate while mechanical properties are varied. In addition, only pure-rolling conditions are considered. Note that, since in this section the thermal properties of the coatings are the same as those of the substrate, the case $E_c = E_s = 210\mathrm{GPa}$ corresponds basically to an uncoated contact case.

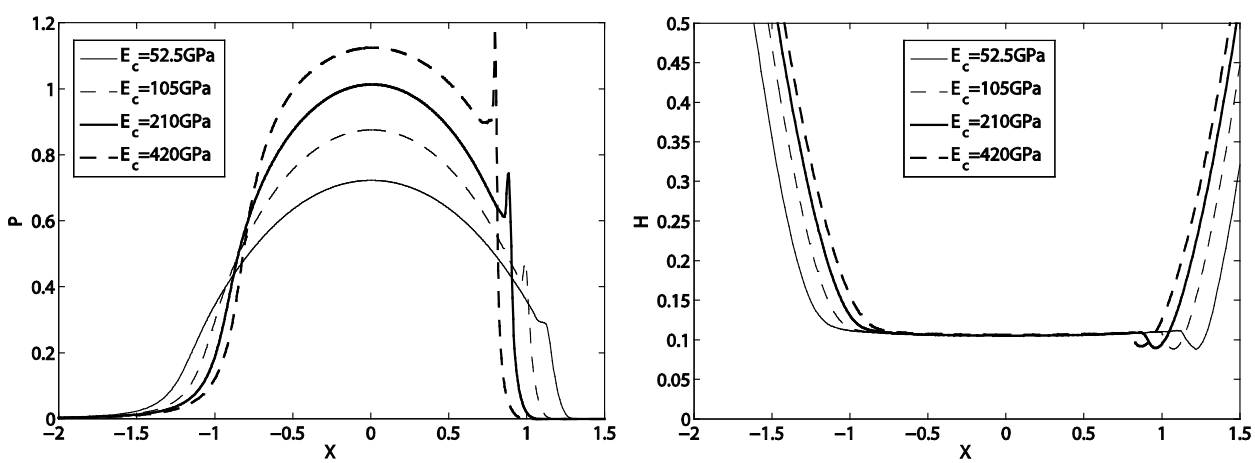

Figure 5: Effect of coating's mechanical properties on dimensionless pressure (left) and lubricant film thickness (right) in coated TEHD circular contacts under pure-rolling conditions (*F*=25N, t_c=40µm, *SRR*=0)

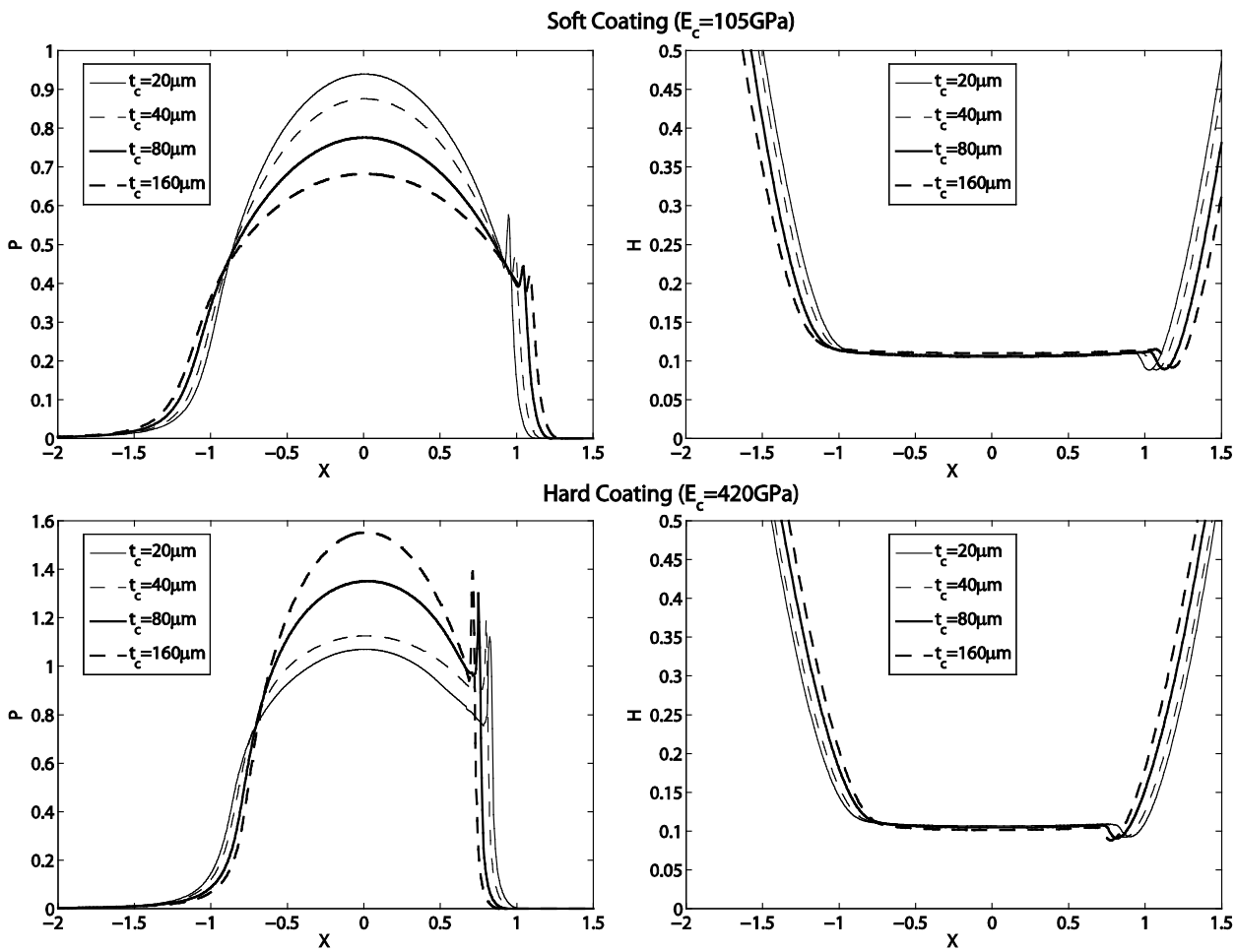

Figure 6: Effect of coating's thickness on dimensionless pressure (left) and lubricant film thickness (right) in coated TEHD circular contacts under pure-rolling conditions (F=25N)

Figures 5 and 6 confirm the classical observations found in the literature (e.g. [7] [9] [10]) pertaining to the effects of the mechanical properties on pressure and film thickness in coated EHL contacts. That is, central pressure and pressure spike height increase with the rigidity of the coating while contact width is reduced. This effect is further emphasized with the increase in coating's thickness as suggested by Figure 6. In fact, for hard coatings, central pressure and pressure spike increase with the thickness of the coating while contact width is reduced. On the other hand, for soft coatings, central pressure and pressure spike decrease with the coating's thickness while contact width increases. Note that in all cases, film thickness is barely affected by the variations in mechanical properties of the coating.

3.2. Effect of coating thermal properties

In this section, the effects of the coating's thermal properties on the lubrication performance of coated circular TEHD contacts are investigated. In the following, the friction coefficient is evaluated at the mid-layer of the lubricant film as:

$$\text{Friction Coefficient} = \frac{\int_{\Omega_c} \tau_{zx}\big|_{Z=0.5} d\Omega}{F}$$
$$\text{with: } \tau_{zx} = \eta\,\dot{\gamma}_{zx} = \frac{\partial p}{\partial x}\left(z - \frac{\eta_e}{\eta_e'}\right) + \eta_e\left(u_b - u_p\right) \tag{21}$$

In order to isolate the effects of the coating's thermal properties, the mechanical properties of the coating are taken to be those of the substrate while the thermal properties are varied. Three categories of coatings are considered based on their thermal properties, more specifically based on their thermal inertia $I = \sqrt{k\,\rho\,c}$. These are: low, regular and high thermal inertia coatings for which thermal inertia is smaller than, equal to or greater than the thermal inertia of the substrate respectively. Note that, since in this section the mechanical properties of the coating are the same as those of the substrate, the case of regular inertia coatings corresponds basically to an uncoated contact case.

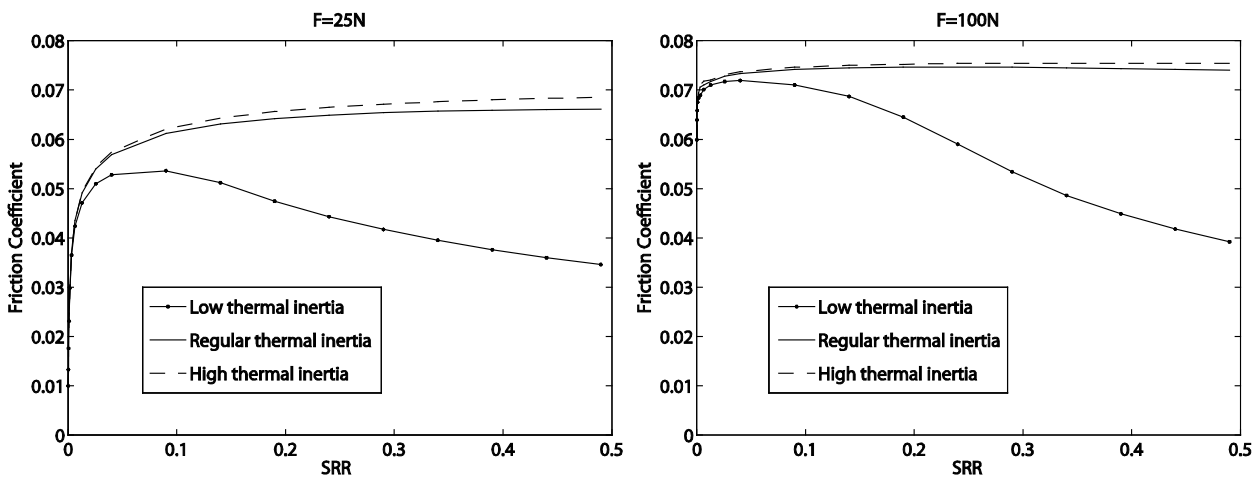

Figure 7: Effect of coating's thermal inertia on friction in coated circular TEHD contacts (t_c=40μm)

Figure 7 suggests that for low thermal inertia coatings, friction is significantly reduced at high *SRR* compared to the case of regular thermal inertia coatings (or the uncoated case). In fact, friction is reduced by a factor of almost 50% at *SRR*=0.5 for both load cases shown in figure 7. On the other hand, high thermal inertia coatings lead to higher friction coefficients compared to the uncoated case. Figure 8 shows the corresponding dimensionless pressure (left) and film thickness (right) profiles along the centerline of the contact in the *x*-direction for the case *F*=25N at *SRR*=0.5. Obviously, both pressure and film thickness distributions are very little affected by the thermal inertia of the coating except in the vicinity of the pressure spike and film thickness constriction respectively.

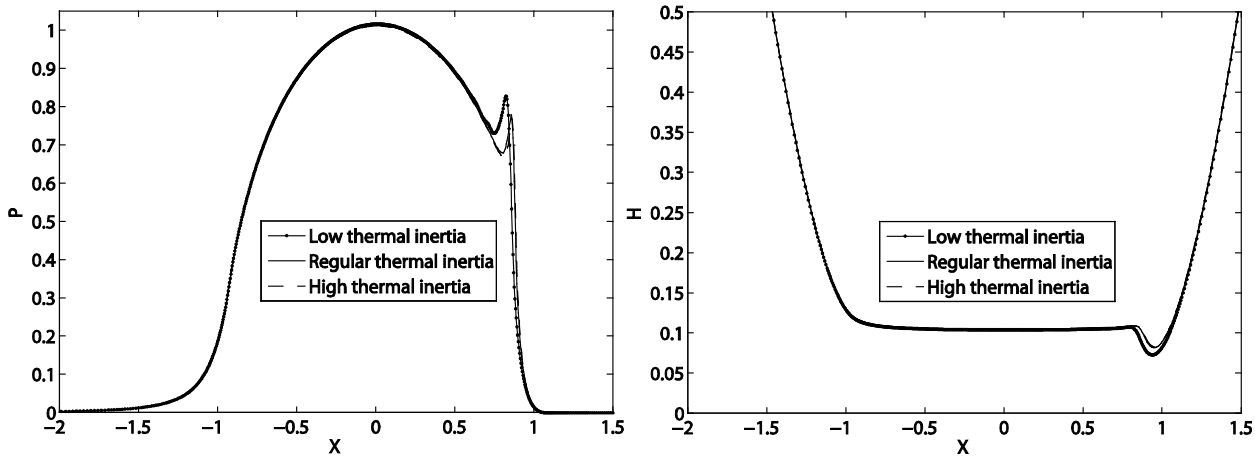

Figure 8: Effect of coating's thermal inertia on dimensionless pressure (left) and lubricant film thickness (right) in coated TEHD circular contacts (F=25N, SRR=0.5, t_c=40μm)

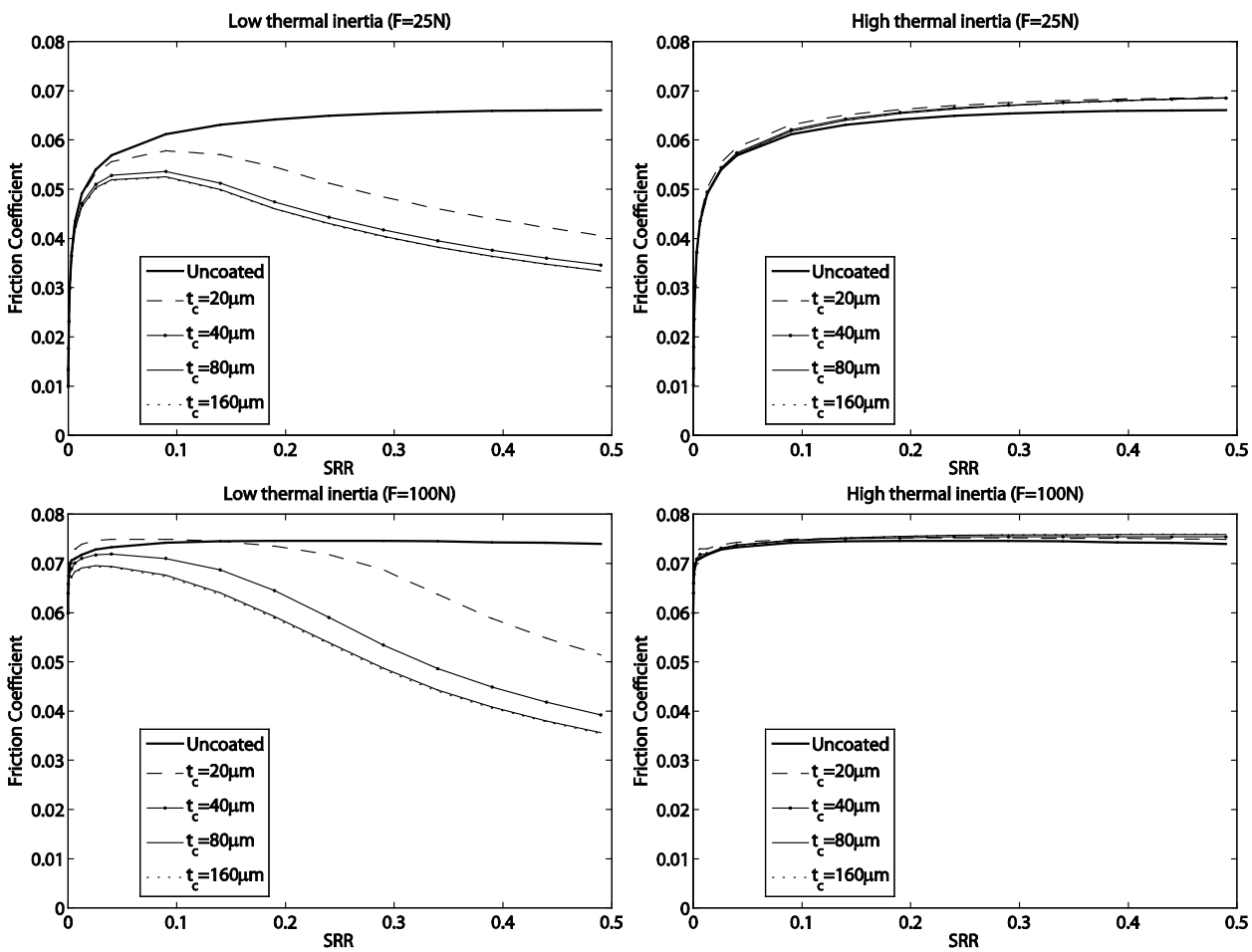

Figure 9: Effect of coating's thickness on friction in coated circular TEHD contacts

Figure 9 suggests that the observations made in figure 7 are further amplified with the increase of the coating's thickness. That is, increasing the coating's thickness for low thermal inertia coatings leads to a more pronounced decrease in friction. However, a limiting value may be noted. In fact, for both loading cases considered in figure 9, it is clear that any increase in the

coating's thickness beyond 80μm has very little effect on friction coefficients. For high thermal inertia coatings on the other hand, increasing the coating's thickness leads to a more pronounced increase in friction. This effect is however barely noticeable for the loading cases considered here for reasons discussed next. Note that, for all cases considered in this section, although friction is significantly affected in some cases, film thickness shows very little deviation from the uncoated case. In fact, for the most extreme case of F=100N, SRR=0.5 and t_c=160μm considered here, the maximum deviation in central film thickness from the uncoated case is of the order of 1%, and for the minimum film thickness it is of the order of 7%.

4. Discussion

The results of the previous section showed that the mechanical properties of the coating in coated TEHD circular contacts had a significant effect on lubricating performance. In fact, it was shown that the central pressure and the height of the pressure spike increase with the rigidity of the coating while the contact's width is reduced and that this effect is amplified with an increase in the thickness of the coating. These observations are rather classical and have been thoroughly discussed in the coated EHL literature. On the other hand, a more interesting observation was made pertaining to the effects of the thermal properties of coatings on friction. That is, friction may be controlled in coated circular TEHD contacts by an adequate choice (based on thermal properties) of surface coatings without any significant impact on film thickness. In fact, it was shown that low thermal inertia coatings may be used to reduce friction while high thermal inertia coatings may be used to increase it under high sliding regime and that these friction variations are amplified with the coating's thickness. These observations are thoroughly discussed in this section, and their origins investigated.

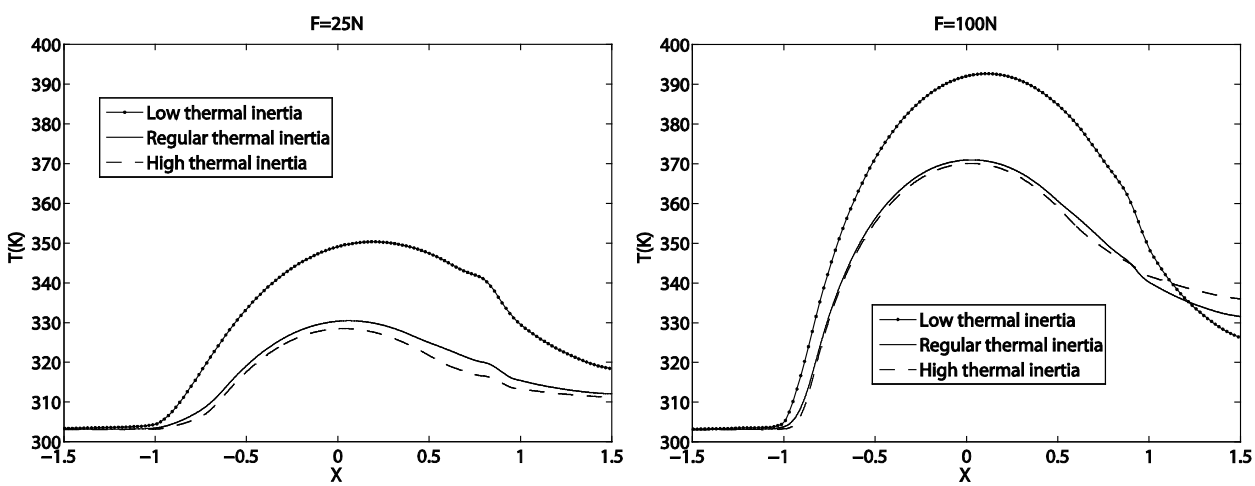

Figure 10: Temperature distribution in coated TEHD circular contacts along the centerline of the contact (Y=0.0) in the mid-layer of the lubricant film (Z=0.5) for the case SRR=0.5 and t_c=40μm. Left: F=25N; right: F=100N

Before providing a physical explanation of the friction variations discussed above in coated TEHD contacts, the reader is reminded that thermal inertia represents the ability of a material to transport heat by conduction and advection and that the regular thermal inertia coating case

discussed in this section corresponds to an uncoated case since both the coating's mechanical and thermal properties are the same as those of the substrate.

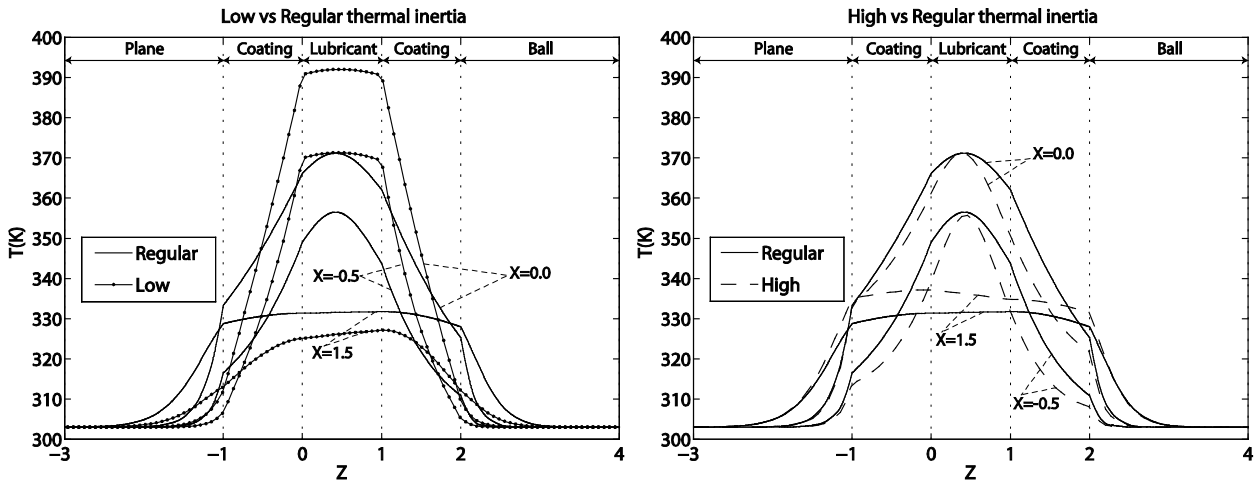

Figure 11: Temperature distribution across the solids (substrates + coatings) and lubricant film in the *Z*-direction at different *X* positions (*X*=-0.5, *X*=0.0 and *X*=1.5) for the case *F*=100N, *SRR*=0.5 and t_c=40μm. Left: Low vs Regular thermal inertia; right: High vs Regular thermal inertia

Figure 10 shows the temperature distribution along the centerline of the contact (*Y*=0.0) in the mid-layer of the lubricant film (*Z*=0.5) for the case *SRR*=0.5 and t_c=40μm for both loading cases considered in the previous section (*F*=25N (left) and *F*=100N (right)). These are the same cases that were previously considered in figure 7. Note that in the central contact region, temperature increases for decreasing thermal inertia of the coating. This comes as no surprise, since heat is generated in the central area of the contact and a low thermal inertia coating would act as an insulator preventing heat from being dissipated towards the peripheral area and the solids. Thus, higher temperatures are observed within the lubricant film in the central region of the contact leading to lower viscosities and thus lower friction. A high thermal inertia coating would have the exact opposite effect. That is, heat is better dissipated towards the peripheral area of the contact and the solids leading to lower temperatures within the lubricant film in the central region and thus higher viscosities and higher friction.

Note that for the case *F*=100N, the temperature trends are inverted towards the contact's exit. That is, lubricant's temperature is higher for higher thermal inertia coatings. This results from heat transfer by conduction and advection within the coating from the center of the contact (where most of the heat is generated) towards the outlet. In fact, high thermal inertia coatings can transport more heat towards the contact's exit which leads to higher solid surface temperatures there, maintaining the lubricant film at a higher temperature. This inversion in temperature trends cannot be observed though for the case *F*=25N. Most likely, this is because the amount of heat generated at the center of the contact for this lower load case, and thus the amount of heat transported towards the outlet by the coatings is not sufficient to invert the temperature trends. Also note that the temperature variations observed in figure 10 remain confined to the central and exit regions of the contact and no significant temperature variations are observed at the

contact's inlet. This explains the minor effect of the thermal properties of the coating on film thickness as discussed in the previous section. In fact, EHL film thickness is known to be governed by the lubricant's rheological behavior in the inlet region of the contact while friction is governed by its rheological response in the central region. Figure 11 shows the temperature distribution across the solids (substrates + coatings) and lubricant film in the *Z*-direction at different *X* positions (*X*=-0.5, *X*=0.0 and *X*=1.5) for the case *F*=100N, *SRR*=0.5 and t_c=40μm discussed in figure 10 (right). Note the faster temperature drop with depth within the coatings with decreasing thermal inertia. This comes as a consequence of the lower ability of lower thermal inertia coatings to dissipate heat by conduction from the lubricant film towards the solids. Also note that the temperature distributions in figure 11 confirm the increased heat transport by the coating towards the exit of the contact (when its thermal inertia is increased) leading to the inversion in temperature trends discussed above.

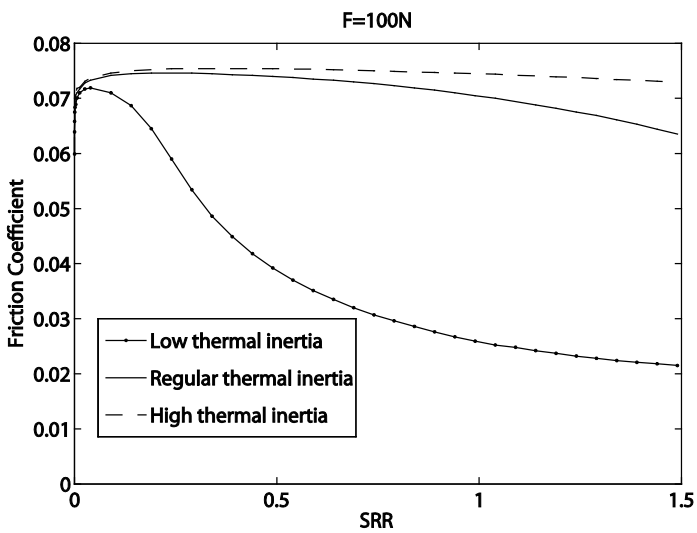

Figure 12: Effect of coating's thermal inertia on friction in coated circular TEHD contacts up to *SRR*=1.5 for the case *F*=100N (t_c=40μm)

Finally, note that all observations made so far pertaining to the coating's thermal properties effects on friction and temperature are barely noticeable for the case of high compared to regular thermal inertia coatings than they are for the case of low compared to regular thermal inertia coatings. The reason is that for the cases considered here, even at the highest sliding speeds (*SRR*=0.5); for the regular thermal inertia case, the friction regime is the "plateau regime" as defined and discussed in [33]. In this regime, friction is governed by the limiting shear stress of the lubricant which smears out all other effects, in particular thermal and viscous ones. When a low thermal inertia coating is used, the significant increase in the lubricant temperature in the central region of the contact leads to lower viscosities, bringing shear stresses below the limiting stress threshold. And the friction regime is now the "thermoviscous regime" [33] in which friction is dictated by the thermal and viscous behaviors of the lubricant rather than the limiting shear stress. This is manifested by a decrease in friction with *SRR* as observed in figure 7 for instance at high *SRR*. When a high thermal inertia coating is used on the other hand, the decrease

in temperature observed in the lubricant film in the central region of the contact, leads to an increase in viscosity and as a consequence in shear stresses. Thus shear stresses in the central region of the contact increase even further above the limiting shear stress threshold and are as a consequence limited to τ_L. Thus, the friction regime remains the "plateau regime" and very little variation is observed in friction as well as in temperature since the limiting shear stress dominates thermal and viscous effects. Increasing the range of *SRR* to 1.5 as shown in figure 12 (for F=100N and t_c=40μm for instance) reveals that friction falls in the "thermoviscous regime" for the regular thermal inertia coating case but remains in the "plateau regime" for the high thermal inertia coating case. As a consequence, the difference in friction between the two cases is no longer insignificant.

5. Conclusion

This paper presents a finite element model for the solution of coated TEHD circular contacts. The effects of the coating's mechanical and thermal properties on the lubrication performance of these contacts are investigated. The effects of the mechanical properties of the coating on pressure and film thickness are consistent with previous findings in the literature. In fact, it is found that the central pressure and the height of the pressure spike increase with the rigidity of the coating while the contact's width is reduced and that this effect is amplified with an increase in the thickness of the coating. However, the main novelty in this work pertains to the effect of the thermal properties of the coating on the frictional response of the contact. It is found that friction may be controlled in TEHD contacts by a suitable choice of surface coating (based on thermal properties) without any significant impact on film thickness. Two categories of surface coatings are considered: high and low thermal inertia. Low thermal inertia surface coatings are found to act as insulators; leading to a localized increase in the lubricant's temperature at the center of the contact. Therefore, friction can be significantly reduced while film thickness is barely affected. The opposite effect is observed for high thermal inertia coatings. That is, the lubricant temperature is decreased at the center of the contact leading to increased friction with very little effect on film thickness. Both effects are found to increase with the thickness of the coating.

Appendix A: Linear elasticity equations

This appendix provides a detailed derivation of the dimensionless linear elasticity equations (5a) and (5b) of the equivalent solid body (substrate + coating) and their associated boundary conditions provided in equation (7). The starting point is the classical three-dimensional linear elasticity equations given below in dimensional form for an elastic material with Lamé parameters λ and μ:

$$\begin{cases} \frac{\partial}{\partial x}\left[(\lambda+2\mu)\frac{\partial u}{\partial x}+\lambda\frac{\partial v}{\partial y}+\lambda\frac{\partial w}{\partial z}\right]+\frac{\partial}{\partial y}\left[\mu\left(\frac{\partial u}{\partial y}+\frac{\partial v}{\partial x}\right)\right]+\frac{\partial}{\partial z}\left[\mu\left(\frac{\partial u}{\partial z}+\frac{\partial w}{\partial x}\right)\right]=0 \\ \frac{\partial}{\partial x}\left[\mu\left(\frac{\partial u}{\partial y}+\frac{\partial v}{\partial x}\right)\right]+\frac{\partial}{\partial y}\left[\lambda\frac{\partial u}{\partial x}+(\lambda+2\mu)\frac{\partial v}{\partial y}+\lambda\frac{\partial w}{\partial z}\right]+\frac{\partial}{\partial z}\left[\mu\left(\frac{\partial v}{\partial z}+\frac{\partial w}{\partial y}\right)\right]=0 \\ \frac{\partial}{\partial x}\left[\mu\left(\frac{\partial u}{\partial z}+\frac{\partial w}{\partial x}\right)\right]+\frac{\partial}{\partial y}\left[\mu\left(\frac{\partial v}{\partial z}+\frac{\partial w}{\partial y}\right)\right]+\frac{\partial}{\partial z}\left[\lambda\frac{\partial u}{\partial x}+\lambda\frac{\partial v}{\partial y}+(\lambda+2\mu)\frac{\partial w}{\partial z}\right]=0 \end{cases} \quad \text{(A.1)}$$

Applying the above equations to the substrate, and writing space coordinates and elastic deformations as a function of their dimensionless equivalents provided in equation (1), the dimensionless form of the linear elasticity equations applied to the substrate is obtained:

$$\begin{cases} \frac{\partial}{a\,\partial X}\left[(\lambda_s+2\mu_s)\frac{a^2}{R\,a}\frac{\partial U}{\partial X}+\lambda_s\frac{a^2}{R\,a}\frac{\partial V}{\partial Y}+\lambda_s\frac{a^2}{R\,a}\frac{\partial W}{\partial Z}\right] \\ \qquad +\frac{\partial}{a\,\partial Y}\left[\mu_s\frac{a^2}{R\,a}\left(\frac{\partial U}{\partial Y}+\frac{\partial V}{\partial X}\right)\right]+\frac{\partial}{a\,\partial Z}\left[\mu_s\frac{a^2}{R\,a}\left(\frac{\partial U}{\partial Z}+\frac{\partial W}{\partial X}\right)\right]=0 \\ \frac{\partial}{a\,\partial X}\left[\mu_s\frac{a^2}{R\,a}\left(\frac{\partial U}{\partial Y}+\frac{\partial V}{\partial X}\right)\right]+\frac{\partial}{a\,\partial Y}\left[\lambda_s\frac{a^2}{R\,a}\frac{\partial U}{\partial X}+(\lambda_s+2\mu_s)\frac{a^2}{R\,a}\frac{\partial V}{\partial Y}+\lambda_s\frac{a^2}{R\,a}\frac{\partial W}{\partial Z}\right] \\ \qquad +\frac{\partial}{a\,\partial Z}\left[\mu_s\frac{a^2}{R\,a}\left(\frac{\partial V}{\partial Z}+\frac{\partial W}{\partial Y}\right)\right]=0 \\ \frac{\partial}{a\,\partial X}\left[\mu_s\frac{a^2}{R\,a}\left(\frac{\partial U}{\partial Z}+\frac{\partial W}{\partial X}\right)\right]+\frac{\partial}{a\,\partial Y}\left[\mu_s\frac{a^2}{R\,a}\left(\frac{\partial V}{\partial Z}+\frac{\partial W}{\partial Y}\right)\right] \\ \qquad +\frac{\partial}{a\,\partial Z}\left[\lambda_s\frac{a^2}{R\,a}\frac{\partial U}{\partial X}+\lambda_s\frac{a^2}{R\,a}\frac{\partial V}{\partial Y}+(\lambda_s+2\mu_s)\frac{a^2}{R\,a}\frac{\partial W}{\partial Z}\right]=0 \end{cases} \quad \text{(A.2)}$$

After simplification, and removing the $1/R$ term common to all terms of the above equations, the system of equations (5a) is obtained:

$$\begin{cases} \frac{\partial}{\partial X}\left[(\lambda_s+2\mu_s)\frac{\partial U}{\partial X}+\lambda_s\frac{\partial V}{\partial Y}+\lambda_s\frac{\partial W}{\partial Z}\right]+\frac{\partial}{\partial Y}\left[\mu_s\left(\frac{\partial U}{\partial Y}+\frac{\partial V}{\partial X}\right)\right]+\frac{\partial}{\partial Z}\left[\mu_s\left(\frac{\partial U}{\partial Z}+\frac{\partial W}{\partial X}\right)\right]=0 \\ \frac{\partial}{\partial X}\left[\mu_s\left(\frac{\partial U}{\partial Y}+\frac{\partial V}{\partial X}\right)\right]+\frac{\partial}{\partial Y}\left[\lambda_s\frac{\partial U}{\partial X}+(\lambda_s+2\mu_s)\frac{\partial V}{\partial Y}+\lambda_s\frac{\partial W}{\partial Z}\right]+\frac{\partial}{\partial Z}\left[\mu_s\left(\frac{\partial V}{\partial Z}+\frac{\partial W}{\partial Y}\right)\right]=0 \\ \frac{\partial}{\partial X}\left[\mu_s\left(\frac{\partial U}{\partial Z}+\frac{\partial W}{\partial X}\right)\right]+\frac{\partial}{\partial Y}\left[\mu_s\left(\frac{\partial V}{\partial Z}+\frac{\partial W}{\partial Y}\right)\right]+\frac{\partial}{\partial Z}\left[\lambda_s\frac{\partial U}{\partial X}+\lambda_s\frac{\partial V}{\partial Y}+(\lambda_s+2\mu_s)\frac{\partial W}{\partial Z}\right]=0 \end{cases} \quad \text{(A.3)}$$

Similarly, applying equations (A.1) to the coating, and writing space coordinates and elastic deformations as a function of their dimensionless equivalents provided in equation (1), the dimensionless form of the linear elasticity equations applied to the coating is obtained:

$$\begin{cases} \dfrac{\partial}{a\,\partial X}\left[\left(\lambda_c+2\mu_c\right)\dfrac{a^2}{R\,a}\dfrac{\partial U}{\partial X}+\lambda_c\dfrac{a^2}{R\,a}\dfrac{\partial V}{\partial Y}+\lambda_c\dfrac{a^2}{R\,t_c}\dfrac{\partial W}{\partial Z}\right] \\ \qquad +\dfrac{\partial}{a\,\partial Y}\left[\mu_c\dfrac{a^2}{R\,a}\left(\dfrac{\partial U}{\partial Y}+\dfrac{\partial V}{\partial X}\right)\right]+\dfrac{\partial}{t_c\,\partial Z}\left[\mu_c\left(\dfrac{a^2}{R\,t_c}\dfrac{\partial U}{\partial Z}+\dfrac{a^2}{R\,a}\dfrac{\partial W}{\partial X}\right)\right]=0 \\ \dfrac{\partial}{a\,\partial X}\left[\mu_c\dfrac{a^2}{R\,a}\left(\dfrac{\partial U}{\partial Y}+\dfrac{\partial V}{\partial X}\right)\right]+\dfrac{\partial}{a\,\partial Y}\left[\lambda_c\dfrac{a^2}{R\,a}\dfrac{\partial U}{\partial X}+\left(\lambda_c+2\mu_c\right)\dfrac{a^2}{R\,a}\dfrac{\partial V}{\partial Y}+\lambda_c\dfrac{a^2}{R\,t_c}\dfrac{\partial W}{\partial Z}\right] \\ \qquad +\dfrac{\partial}{t_c\,\partial Z}\left[\mu_c\left(\dfrac{a^2}{R\,t_c}\dfrac{\partial V}{\partial Z}+\dfrac{a^2}{R\,a}\dfrac{\partial W}{\partial Y}\right)\right]=0 \\ \dfrac{\partial}{a\,\partial X}\left[\mu_c\left(\dfrac{a^2}{R\,t_c}\dfrac{\partial U}{\partial Z}+\dfrac{a^2}{R\,a}\dfrac{\partial W}{\partial X}\right)\right]+\dfrac{\partial}{a\,\partial Y}\left[\mu_c\left(\dfrac{a^2}{R\,t_c}\dfrac{\partial V}{\partial Z}+\dfrac{a^2}{R\,a}\dfrac{\partial W}{\partial Y}\right)\right] \\ \qquad +\dfrac{\partial}{t_c\,\partial Z}\left[\lambda_c\dfrac{a^2}{R\,a}\dfrac{\partial U}{\partial X}+\lambda_c\dfrac{a^2}{R\,a}\dfrac{\partial V}{\partial Y}+\left(\lambda_c+2\mu_c\right)\dfrac{a^2}{R\,t_c}\dfrac{\partial W}{\partial Z}\right]=0 \end{cases} \tag{A.4}$$

After simplification, and multiplying all the above equations by $R\,t_c/a$, the system of equations (5b) is obtained:

$$\begin{cases} \dfrac{\partial}{\partial X}\left[\left(\lambda_c+2\mu_c\right)\dfrac{t_c}{a}\dfrac{\partial U}{\partial X}+\lambda_c\dfrac{t_c}{a}\dfrac{\partial V}{\partial Y}+\lambda_c\dfrac{\partial W}{\partial Z}\right] \\ \qquad +\dfrac{\partial}{\partial Y}\left[\mu_c\dfrac{t_c}{a}\left(\dfrac{\partial U}{\partial Y}+\dfrac{\partial V}{\partial X}\right)\right]+\dfrac{\partial}{\partial Z}\left[\mu_c\left(\dfrac{a}{t_c}\dfrac{\partial U}{\partial Z}+\dfrac{\partial W}{\partial X}\right)\right]=0 \\ \dfrac{\partial}{\partial X}\left[\mu_c\dfrac{t_c}{a}\left(\dfrac{\partial U}{\partial Y}+\dfrac{\partial V}{\partial X}\right)\right]+\dfrac{\partial}{\partial Y}\left[\lambda_c\dfrac{t_c}{a}\dfrac{\partial U}{\partial X}+\left(\lambda_c+2\mu_c\right)\dfrac{t_c}{a}\dfrac{\partial V}{\partial Y}+\lambda_c\dfrac{\partial W}{\partial Z}\right] \\ \qquad +\dfrac{\partial}{\partial Z}\left[\mu_c\left(\dfrac{a}{t_c}\dfrac{\partial V}{\partial Z}+\dfrac{\partial W}{\partial Y}\right)\right]=0 \\ \dfrac{\partial}{\partial X}\left[\mu_c\left(\dfrac{\partial U}{\partial Z}+\dfrac{t_c}{a}\dfrac{\partial W}{\partial X}\right)\right]+\dfrac{\partial}{\partial Y}\left[\mu_c\left(\dfrac{\partial V}{\partial Z}+\dfrac{t_c}{a}\dfrac{\partial W}{\partial Y}\right)\right] \\ \qquad +\dfrac{\partial}{\partial Z}\left[\lambda_c\dfrac{\partial U}{\partial X}+\lambda_c\dfrac{\partial V}{\partial Y}+\left(\lambda_c+2\mu_c\right)\dfrac{a}{t_c}\dfrac{\partial W}{\partial Z}\right]=0 \end{cases} \tag{A.5}$$

Finally, equations (A.3) and (A.5) are associated with the following boundary conditions, written in dimensional form:

$$\begin{cases} \sigma_{\mathrm{n}} = \sigma \cdot \vec{n} = \sigma_{zz} = \lambda_c \dfrac{\partial u}{\partial x} + \lambda_c \dfrac{\partial v}{\partial y} + \left(\lambda_c + 2\mu_c\right) \dfrac{\partial w}{\partial z} = -p & \text{on } \Omega_{\mathrm{c}} \\ u = v = w = 0 & \text{on } \partial\Omega_{\mathrm{b}} \\ v = 0 & \text{on } \partial\Omega_{\mathrm{s}} \text{ (Symmetry)} \\ \sigma_{\mathrm{n}} = 0 & \text{elsewhere} \end{cases} \tag{A.6}$$

Writing space coordinates and elastic deformations as a function of their dimensionless equivalents provided in equation (1), the dimensionless form of the above boundary conditions is obtained:

$$\begin{cases} \sigma_{\mathrm{n}} = \sigma \cdot \vec{n} = \sigma_{zz} = \lambda_c \dfrac{a^2}{R\,a} \dfrac{\partial U}{\partial X} + \lambda_c \dfrac{a^2}{R\,a} \dfrac{\partial V}{\partial Y} + \left(\lambda_c + 2\mu_c\right) \dfrac{a^2}{R\,t_c} \dfrac{\partial W}{\partial Z} = -P\,p_h & \text{on } \Omega_{\mathrm{c}} \\ \dfrac{a^2}{R} U = \dfrac{a^2}{R} V = \dfrac{a^2}{R} W = 0 & \text{on } \partial\Omega_{\mathrm{b}} \\ \dfrac{a^2}{R} V = 0 & \text{on } \partial\Omega_{\mathrm{s}} \text{ (Symmetry)} \\ \sigma_{\mathrm{n}} = 0 & \text{elsewhere} \end{cases} \tag{A.7}$$

After simplification and rearranging the above first boundary condition, the boundary conditions provided in equation (7) in dimensionless from are obtained:

$$\begin{cases} \bar{\sigma}_{\mathrm{n}} = \bar{\sigma} \cdot \vec{n} = \bar{\sigma}_{ZZ} = \lambda_c \dfrac{\partial U}{\partial X} + \lambda_c \dfrac{\partial V}{\partial Y} + \left(\lambda_c + 2\mu_c\right) \dfrac{a}{t_c} \dfrac{\partial W}{\partial Z} = -\dfrac{P\,R\,p_h}{a} & \text{on } \Omega_{\mathrm{c}} \\ U = V = W = 0 & \text{on } \partial\Omega_{\mathrm{b}} \\ V = 0 & \text{on } \partial\Omega_{\mathrm{s}} \text{ (Symmetry)} \\ \bar{\sigma}_{\mathrm{n}} = 0 & \text{elsewhere} \end{cases} \tag{A.8}$$

Note that in equations (A.3) and (A.5) the continuity of stresses across the substrate-coating interface is automatically satisfied by removing the boundary integral terms that would arise in the weak from finite element formulation at this interface. Also note that the natural boundary condition provided in the first equation of (A.8) is also automatically imposed by setting the value of $\bar{\sigma}_{\mathrm{n}}$ to $-P\,R\,p_h/a$ in the boundary integral term that would arise in the weak form finite element formulation of the last equation in (A.5).

Nomenclature

η	: Lubricant's Generalized Newtonian viscosity (Pa.s)
$\bar{\eta}$	: Dimensionless lubricant's Generalized Newtonian viscosity
λ_c, μ_c	: Coating's Lamé parameters (Pa)
λ_s, μ_s	: Substrate's Lamé parameters (Pa)

μ	: Lubricant's viscosity (Pa.s)
μ_R	: Lubricant's viscosity at reference state (Pa.s)
μ_∞	: Lubricant's viscosity extrapolated to infinite temperature (Pa.s)
υ_c	: Coating's Poisson coefficient
$\upsilon_{c,eq}$	: Coating's equivalent Poisson coefficient
υ_s	: Substrate's Poisson coefficient
$\upsilon_{s,eq}$	: Substrate's equivalent Poisson coefficient
Λ	: Limiting stress-pressure coefficient
ρ	: Lubricant's density (kg/m^3)
$\bar{\rho}$	: Dimensionless lubricant's density
ρ_c	: Coating's density (kg/m^3)
ρ_s	: Substrate's density (kg/m^3)
ρ_R	: Lubricant's density at reference state (kg/m^3)
θ	: Modified dimensionless Hertzian pressure
τ	: Shear stress (Pa)
τ_L	: Limiting shear stress (Pa)
a	: Hertzian contact radius (m)
c	: Lubricant's heat capacity (J/kg.K)
c_c	: Coating's heat capacity (J/kg.K)
c_s	: Substrate's heat capacity (J/kg.K)
C	: Lubricant's volumetric heat capacity (J/m^3.K)
E_c	: Coating's Young's modulus of elasticity (Pa)
$E_{c,eq}$	: Coating's equivalent Young's modulus of elasticity (Pa)
E_s	: Substrate's Young's modulus of elasticity (Pa)
$E_{s,eq}$	: Substrate's equivalent Young's modulus of elasticity (Pa)
F	: Contact external applied load (N)
G	: Lubricant effective shear modulus (Pa)
h	: Lubricant film thickness (m)
H	: Dimensionless lubricant film thickness
H_0	: Film thickness constant parameter
k	: Lubricant's thermal conductivity (W/m.K)
k_c	: Coating's thermal conductivity (W/m.K)
k_s	: Substrate's thermal conductivity (W/m.K)
p	: Pressure (Pa)
P	: Dimensionless pressure
p_h	: Hertzian contact pressure (Pa)
p_0	: Ambient pressure (Pa)
p_R	: Reference pressure (Pa)
R	: Ball's radius (m)
SRR	: Slide-to-Roll ratio = $(u_b-u_p)/u_m$

t_c	: Coating's thickness (m)
T	: Temperature (°C)
T_0	: Ambient temperature (°C)
T_R	: Reference temperature (°C)
u, v, w	: x, y and z-components of the solid's elastic deformation field (m)
U, V, W	: Dimensionless x, y and z-components of the solid's elastic deformation field
u_m	: Mean entrainment speed = $(u_b+u_p)/2$ (m/s)
u_b	: Ball's surface velocity (m/s)
u_p	: Plane's surface velocity (m/s)
u_f, v_f	: Lubricant's velocity field x and y components (m/s)
V	: Volume (m^3)
V_R	: Volume at reference state (m^3)
x, y, z	: Space coordinates (m)
X, Y, Z	: Dimensionless space coordinates

Subscipts

b	: Ball
c	: Coating
p	: Plane
s	: Substrate

References

[1] Bennett A. and Higginson G. R. – Hydrodynamic Lubrication of Soft Solids, *J. Mech. Eng. Sci.*, 1970, vol. 12 (3), pp. 218-222.

[2] Elsharkawy A. A. and Hamrock B. J. – EHL of Coated Surfaces: Part I – Newtonian Results, *ASME Journal of Tribology*, 1994, vol. 116, pp. 29-36.

[3] Elsharkawy A. A. and Hamrock B. J. – EHL of Coated Surfaces: Part II – Non-Newtonian Results, *ASME Journal of Tribology*, 1994, vol. 116, pp. 786-793.

[4] Hlaváček M. – A Central Film Thickness Formula for Elastohydrodynamic Lubrication of Cylinders with Soft Incompressible Coatings and a Non-Newtonian Piecewise Power-Law Lubricant in Steady Rolling Motion, *Wear*, 1997, vol. 205, pp. 20-27.

[5] Jin. Z. M. – Elastohydrodynamic Lubrication of a Circular Point Contact for a Compliant Layered Surface Bonded to a Rigid Substrate, Part 1: Theoretical Formulation and Numerical Method, *IMechE J. Eng. Trib.*, 2000, vol. 214 (3), pp. 267-279.

[6] Jin. Z. M. – Elastohydrodynamic Lubrication of a Circular Point Contact for a Compliant Layered Surface Bonded to a Rigid Substrate, Part 2: Numerical Results, *IMechE J. Eng. Trib.*, 2000, vol. 214 (3), pp. 281-289.

[7] Elsharkawy A. A., Holmes M. J. A., Evans H. P. and Snidle R. W. – Micro-Elastohydrodynamic Lubrication of Coated Cylinders Using Coupled Differential Deflection Method, *IMechE J. Eng. Trib.*, 2006, vol. 220, pp. 29-41.

[8] Holmes M. J. A., Evans H. P., Hughes T. G. and Snidle R. W. - Transient Elastohydrodynamic Point Contact Analysis Using a New Coupled Differential Deflection Method, Part 1: Theory and Validation, *IMechE J. Eng. Trib.*, 2003, vol. 217, pp. 289-303.

[9] Liu Y., Wayne Chen W., Zhu D., Liu S. and Jane Wang Q. – An Elastohydrodynamic Lubrication Model for Coated Surfaces in Point Contacts, *ASME Journal of Tribology*, 2007, vol. 129, pp. 509-516.

[10] Liu Y., Jane Wang Q. and Zhu D. – Effect of Stiff Coatings on EHL Film Thickness in Point Contacts, *ASME Journal of Tribology*, 2008, vol. 130, 031501.

[11] Liu S. B., Wang Q. and Liu G. – A Versatile Method of Discrete Convolution and FFT (DC-FFT) for Contact Analyses, *Wear*, 2000, vol. 243, pp. 101-110.

[12] Evans R. D., Cogdell J. D., and Richter G. A. - Traction of Lubricated Rolling Contacts Between Thin-Film Coatings and Steel, *Tribology Transactions*, 2009, vol. 52 (1), pp. 106–113.

[13] Björling M., Isaksson P., Marklund P. and Larsson R. – The Influence of DLC Coating on EHL Friction Coefficient, *Tribology Letters*, 2012, vol. 47, pp. 285-294.

[14] Björling M., Habchi W., Bair S., Larsson R. and Marklund P. - Friction Reduction in Elastohydrodynamic Contacts by Thin Layer Thermal Insulation, *Tribology Letters*, (In Press).

[15] Habchi. W., Eyheramendy D., Bair S., Vergne P. and Morales-Espejel G. – Thermal Elastohydrodynamic Lubrication of Point Contacts Using a Newtonian / Generalized Newtonian Lubricant, *Tribology Letters*, 2008, vol. 30 (1), pp. 41-52.

[16] Habchi W., Eyheramendy D., Vergne P. and Morales-Espejel G. – Stabilized Fully-Coupled Finite Elements for Elastohydrodynamic Lubrication Problems, *Advances in Engineering Software*, 2012, vol. 46, pp. 4-18.

[17] Yang P. and Wen S. - A Generalized Reynolds Equation for Non-Newtonian Thermal Elastohydrodynamic Lubrication, *ASME Journal of Tribology*, 1990, vol. 112, pp. 631-636.

[18] Hamrock B.J. and Dowson D. - Isothermal elastohydrodynamic lubrication of point contacts. Part I – Theoretical formulation. ASME Journal of Lubrication Technology 1976; vol. 98 (2), pp. 223–229.

[19] Wu S. R. – A Penalty Formulation and Numerical Approximation of the Reynolds-Hertz Problem of Elastohydrodynamic Lubrication, *Int. J. Engnrng. Sci.*, 1986, vol. 24 (6), pp. 1001-1013.

[20] Kaneta M., Shigeta T. and Yang P. – Film Pressure Distributions in Point Contacts Predicted by Thermal EHL Analysis, *Tribology International*, 2006, vol. 39, pp. 812-819.

[21] Wang Y., Li H., Tong J. and Yang P. – Transient Thermoelastohydrodynamic Lubrication Analysis of an Involute Spur Gear, *Tribology International*, 2004, vol. 37, pp. 773-782.

[22] Cheng H. S. - A Refined Solution to the Thermal-Elastohydrodynamic Lubrication of Rolling and Sliding Cylinders. *ASLE Trans.*, 1965, vol. 8, pp. 397-410.

[23] Kim H. J., Ehret P., Dowson D. and Taylor C. M. - Thermal Elastohydrodynamic Analysis of Circular Contacts, Part 2: Non-Newtonian Model, *Proc. IMechE. J. Engnrng. Tribol.*, 2001, Part J., vol. 215, pp. 353-362.

[24] Lin T. R. and Lin J. F. – Thermal Effects in Elastohydrodynamic Lubrication of Line Contacts Using a Non-Newtonian Lubricant. *Tribology International*, 1991, vol. 24, n° 6, pp. 365-372.

[25] Guo F., Yang P. and Qu S. - On the Theory of Thermal Elastohydrodynamic Lubrication at High Slide-Roll Ratios – Circular Glass-Steel Contact Solution at Opposite Sliding. *ASME J. of Tribol.*, 2001, vol. 123, pp. 816-821.

[26] Habchi W., Vergne P., Bair S., Andersson O., Eyheramendy D. and Morales-Espejel G. E. – Influence of Pressure and Temperature Dependence of Thermal Properties of a Lubricant on the Behaviour of Circular TEHD Contacts, *Tribology International*, 2010, vol. 43, pp. 1842-1850.

[27] Habchi W., Vergne P., Fillot N., Bair S. and Morales-Espejel G. E. – A Numerical Investigation of Local Effects on the Global Behavior of TEHD Highly Loaded Circular Contacts, *Tribology International*, 2011, vol. 44, pp. 1987-1996.

[28] COMSOL Multiphysics, *COMSOL Multiphysics Modeling Guide*, COMSOL Inc. (www.comsol.com).

[29] Murnaghan F. D. - The Compressibility of Media under Extreme Pressures, *Proceedings of the National Academy of Sciences*, 1944, vol. 30, p. 244-247.

[30] Vogel H. – The Temperature Dependence Law of the Viscosity of Fluids, *Physikalische Zeitschrift*, 1921, vol. 22, pp. 645-646.

[31] Bair S. – High Pressure Rheology for Quantitative Elastohydrodynamics, Elsevier Science, Amsterdam, 2007.

[32] Bair S. - A Rough Shear Thinning Correction for EHD Film Thickness, *STLE Tribology Trans*., 2004, vol. 47, pp. 361-365.

[33] Habchi W., Bair S. and Vergne P. – On Friction Regimes in Quantitative Elastohydrodynamics, *Tribology International*, 2013, vol. 58, pp. 107-117.